RSC Advances

ROYAL SOCIETY OF CHEMISTRY

www.rsc.org/advances

Table of contents entry

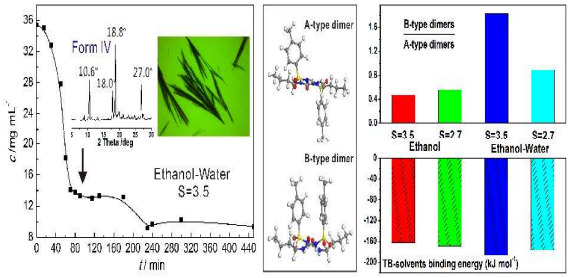

Synopsis

The combined experimental and molecular dynamics simulation study discloses the effects of solvents and supersaturations on tolbutamide polymorphs outcome.

Mechanistic Insight into the Selective Crystallization of the Metastable Polymorph of Tolbutamide in Ethanol-water Solution

Jinli Zhang, Yujia Wu, Anyuan Liu, Wei Li, You Han*

School of Chemical Engineering & Technology, Tianjin University, Tianjin 300072, People's Republic of China

* To whom correspondence should be addressed.

Dr. You Han

Associate Professor

School of Chemical Engineering and Technology,

Tianjin University

92 Weijin Road, Tianjin 300072, china

Tel: +86-22-27401476

Fax: +86-22-27403389

E-mail: yhan@tju.edu.cn

ABSTRACT: The rapid-cooling crystallization of tolbutamide (TB) was carried out from ethanol and ethanol-water solutions at different initial supersaturations (3.5 and 2.7). PXRD and FTIR were used to characterize the polymorphs. It is found that the metastable Form IV with advanced solubility and bioavailability was obtained in ethanol-water solutions at higher supersaturation. While stable Form III directly crystallized from ethanol at both supersaturations and ethanol-water solution at lower supersaturation. Hirshfeld surface and the associated 2D fingerprint plots of five TB polymorphs clearly quantify the interactions within the crystal structures. The mechanism of the selective crystallization of the metastable polymorph of tolbutamide in ethanol-water solution was disclosed by molecular dynamics simulation. It is indicated that stronger interactions between TB and solvents weaken the TB-TB intermolecular NH $\cdots$ O hydrogen bonds and thus promote TB molecules to form dimers by $\pi \cdots \pi$ stacking. This work provides a feasible approach combining the experimental with molecular dynamics simulation methods to understand deeply the effects of solvents and supersaturations on polymorphs outcome by studying competitive relationship between solute-solute and solute-solvent interaction, which is fundamental to the rational design of experimental work on controlling organic crystal polymorphs by simply varying solvents and supersaturations.

KEYWORDS: tolbutamide, molecular dynamics simulation, polymorph, crystallization, solvent, supersaturation.

1. INTRODUCTION

Polymorphism is the feature of a substance to exist two or more crystalline phases that have different arrangements of the molecules in the crystal lattice. Though chemically identical, different polymorphs exhibit distinct physic-chemical properties, such as stability, solubility and bioavailability,[1, 2] which can affect the performance of the drug. Therefore, it is significant to understand the mechanism of polymorphic nucleation in order to selectively obtain the desired polymorph with advanced solubility and bioavailability in pharmaceuticals.

The crystallization process of polymorphs is composed of the competitive nucleation and growth. This process is influenced by various operational factors of crystallizations, such as temperature[3, 4], supersaturation[5-7], solvents[8-10], seeding[11, 12] and additives[13-15]. In solution crystallization, as the first step in the formation of a crystal, nucleation can lead the way to different arrangements of atoms, ions and/or molecules in the solid state[16] and therefore plays a decisive role in determining the crystal structure. However, it is difficult to separate nucleation from the growth process in the experimental studies[17] and the nucleation mechanism of polymorphs under different conditions is still elusive. With the advantages of tracking the motion of each atom, molecular dynamics (MD) simulation has been used widely to investigate the molecular self-assembly in the prenucleation process.[18-21] For instance, the effect of different solvents on the initial association of 5-fluorouracil has been studied by MD simulation and the simulation results provided an explanation for experimental observation[18]. Interaction between tetrolic acid and solvent molecules

has been proved to play an important role in solute self-assembly process, which has a major effect on the polymorphic outcome[19]. The link hypothesis that there exists a link between the growth synthon formed in solution and the structural synthon packed in the crystal can successfully explain crystal output of many systems, such as glycine[22], 2,6-dihydroxylbenzoicacid[23], and tetrolic acid[19]. Hence, it is vital to study intensively how the crystallization conditions affect the interaction between solute and solvents as well as the solute self-assembly in the initial nucleation process by MD simulation, which may facilitate the rational design of experimental work on selective crystallization of polymorphic drugs through the combination of experimental data and molecular modeling methods.

In this work, tolbutamide (1-butyl-3-(4-methylphenylsulfonyl) urea, TB) was selected as a model system, which is an oral hypoglycemic agent and used in the treatment towards insulin-dependent diabetic patients. The molecular structure of TB is shown in Figure 1. According to the reported literature, as a representative case of conformational polymorphism, TB crystallizes in five polymorphic forms[24-27] (see Table S1 in supporting information), which differ in their mode of packing and in molecular conformation but with similar hydrogen bonding synthon. In 2010, the X-ray crystal structures of Form I-IV were solved by Tan and coworkers,[26] and in the next year, novel Form V was accidentally discovered in an attempt to cocrystallize TB.[27]

(Fig. 1)

The metastable Form IV of TB has an enhanced bioavailability compared with

the stable forms (the order of bioavailability: Form IV > Form II > Form III > Form I[28]), thus there is a need to obtain the metastable form from crystallization with proper and easy method. Uekama and coworkers reported the selective crystallization of a metastable Form IV of TB by the complexation with 2,6-di-O-methyl-β-cyclodextrin[29]. Our previous study[28] introduced the method of controlling TB polymorphs by self-assembled monolayers.

In the present study, the metastable Form IV of TB has successfully crystallized from TB solution via simply controlling the supersaturation and solvent factors. The molecular dynamics simulations combined with experimental characterization methods have been used to further investigate the effect mechanism of supersaturation and solvent on the TB nucleation process. This work provides a feasible approach combining the experimental with molecular modeling methods to understand deeply the role of prenucleation molecular self-assembly in polymorph outcome and the relationship between the crystallization conditions and the selective crystallization of polymorphic drugs.

2. EXPERIMENTAL AND MODELING METHODS

2.1. Experimental Materials. TB (≥98%) was purchased from Reihefeng Technology & Trade Co., Ltd, and used without further purification. The powder X-ray diffraction (PXRD) data and differential scanning calorimetry (DSC) analysis of TB confirms that it belongs to Form I. As the solvents for crystallization, we selected ethanol (polar-protic) and ethanol-water (*v*: *v* = 2:1) (polar-aprotic). These solvents (ethanol and deionized water) were of analytical reagent grade and were

purchased from Binhai Chemical Plant, Tianjin.

2.2. TB crystallization. The crystallization of TB was carried out by the rapid-cooling method in ethanol and ethanol-water solutions. The solubility of TB in ethanol and ethanol-water solvents at 277 K were determined via the balance method using a UV-Vis spectrophotometer[30], and it was 44.56 mg/mL and 10.10 mg/mL, respectively. Various supersaturations (2.7 and 3.5 at 277 K) of TB crystals were dissolved in solvents in a 20 ml crystallization vessel at 303 K. After complete dissolution, the solution was filtered through a millipore (0.22 μm) syringe filter and rapidly cooled to 277 K in a thermostat (refrigerator). The liquid-phase samples (from the same batch) were removed at constant time intervals by a pipette, diluted and analyzed by UV spectroscopic methods[29] for the TB solute concentration measurement until the final concentration reached relatively stable values.

2.3. Characterization. The solid-phase of TB crystallized from ethanol and ethanol-water solution at different supersaturation (2.7 and 3.5) were collected by filtration method and then dried at 298K for 24 h. Then, they were subjected to the PXRD and Fourier transform infrared spectroscopy (FTIR) to identify the form of the crystal.

The PXRD patterns of crystallized TB were collected for phase identification with a scanning speed 3° /min on a Rigaku Geigerflex D/MAX 2500 v/PC diffractometer with Cu Kα radiation at 40 kV.

The FTIR analyses of the crystals were performed on Thermo Nicolet IZ10 with DTGS detector and OMNIC version 8.0 was used for operation. A total of 32 scans

were collected over the range of 400-4000 cm^{-1}, with a resolution of 4 cm^{-1} for each FTIR spectrum.

Meanwhile, morphologies of TB crystals were observed using a polarizing microscope (Sunny Optical Technology XY-P) equipped with a CCD color camera (YESONE, CS080).

2.4. Hirshfeld Surface Analysis. Molecular Hirshfeld surfaces in the crystal structure are constructed based on the electron distribution calculated as the sum of spherical atom electron densities.[31, 32] The Hirshfeld surfaces are mapped with d_{norm} (the normalized contact distance) and their associated 2D fingerprint plots presented in this paper were generated using CrystalExplorer 3.1.[33] Bond lengths to hydrogen atoms were set to typical neutron values (C-H = 1.083 Å, O-H= 0.983 Å, N-H = 1.009 Å).

2.5. Molecular Dynamics Details of TB Nucleation. TB crystal structure were directly obtained from Cambridge Structural Database(CSD), namely, ZZZPUS04, ZZZPUS05, ZZZPUS06, ZZZPUS07[26] and ZZZPUS10[27] corresponding to polymorphs I–V, respectively. The disordered alkyl chain of one TB molecule Ch4 in Form II was remodeled, considering the atoms with greater occupancy only.

In order to determine a suitable force field to model TB during the dynamics simulation process, three force fields (cvff [34], COMPASS and dreiding force field) were tested. It is found that the use of cvff force field showed better performance for the percentage changes of lattice parameters and the root mean squared difference calculation. In addition, cvff force field was suitable for water-containing systems[35]

and a wide range of organic systems. Thus, it was adopted in all calculations in the following studies.

The aggregation behavior of the TB molecules in various solutions was studied by means of MD simulations, under Periodic Boundary Conditions, using the Forcite module as implemented in Materials Studio 5.0 software from Accelrys. The TB monomer was obtained from Form I crystal, consistent with the dissolution of Form I crystal in solvents. The molecules of TB, ethanol and water were initially geometry optimized in DMol^3 Module. The initial simulation boxes were constructed with properties which are summarized in Table 1. There were 16, 12, 8 and 6 TB molecules, 484 , 488, 700 and 680 ethanol molecules, along with 0, 0, 1132 and 1102 water molecules for the system of S_e=3.5, S_e=2.7, $S_{e\text{-}w}$=3.5 and $S_{e\text{-}w}$=2.7 (corresponding to initial TB concentration of 155.97, 120.32, 35.36 and 27.28 mg/mL), respectively. The systems were first geometry optimized to remove accidental overlapping of the molecules. The equilibration period was 500 ps, during which all the molecules were free to move in the NVT ensemble (constant number of particles, volume and temperature). The temperature was fixed at 303 K using Nose[36] thermostat which corresponded to the experimental temperature of dissolution of TB in solvents. We then simulated the systems for 4 ns in the NPT ensemble(constant number of particles, pressure and temperature), using Nose thermostat and Berendsen barostat methods to maintain temperature at 277 K and pressure at 1atm. Electrostatic interaction and van der Waals interaction were calculated using Ewald method[37]. The time step used to solve the equations of motion was 1 fs. Only the last 1 ns of simulation were used for

production of results. Since all molecules are flexible in the simulation, we calculated the torsion distribution of seven torsion angles of TB molecules in solution. Because of the limitations of simulation time and system size, it is difficult to observe the formation of large organic clusters in solutions.[18, 21, 38, 39] Therefore, only the initial stage of TB nucleation was investigated in our simulations.

(Table 1)

The binding energy of TB dimers in vaccum was calculated, which was defined as:

$$\Delta E_{\text{binding (TB-TB)}} = E_{\text{dimer}} - 2E_{\text{TB}}$$

where E_{dimer} is the energy of the TB dimers, and E_{TB} is the energy of one TB molecule alone.

The binding energy of TB and solvents was defined as:

$$\Delta E_{\text{binding (TB-S)}} = \frac{1}{N}(E_{\text{total}} - E_{\text{TB}} - E_{\text{solvent}})$$

where E_{total} is the total energy of the TB molecules and the solvents, E_{solvent} and E_{TB} are the energies of the solvents and TB molecules, respectively. N is the number of TB molecules in the models.

The TB-TB aggregation and TB-solvent interaction were further studied by analyzing the radial distribution functions (RDFs) of different sets of atoms, $g_{\alpha\beta}(r)$, which describes how the particle density of a system varies with a distance, measured from a reference particle. To obtain the quantitative insight on the RDF plots, the coordination number was calculated according to the following equation[40]:

$$N_{\alpha(\beta)}(r) = 4\pi \int_{r0}^{r1} r^2 g_{\alpha\beta}(r) \rho \mathrm{d}r$$

where $N_{\alpha(\beta)}(r)$ is the number of β species surrounding α at less than a given distance, ρ

is the bulk number density of atom β and $g_{\alpha\beta}(r)$ is the α-β RDF.

3. RESULTS AND DISCUSSION

3.1. TB crystallization from ethanol and ethanol-water. The rapid cooling crystallization of TB from ethanol and ethanol-water was performed respectively. Figure 2 shows the changes in the concentration of TB in the solution during each run. For crystallization of TB from ethanol, the initial concentrations of the solution were 155.97 mg/mL and 120.32 mg/mL which correspond to the TB supersaturation of 3.5 and 2.7 in ethanol at 277 K. The TB concentration, detected by UV absorption at 229nm, decreased with time, indicative of nucleation and growth of crystals. In both cases, after a decrease in TB concentration due to crystallization, the concentration attained a constant value of about 43.60 mg/mL (Fig. 2a). The induction time of crystallization at lower supersaturation system is obviously longer than that of higher supersaturation system. Similarly, crystallization of TB was conducted in ethanol-water solutions at initial concentration of 35.36 mg/mL ($S_{e\text{-}w}$=3.5) and 27.28 mg/mL ($S_{e\text{-}w}$=2.7). TB concentration profiles under both conditions are shown in Figure 2b. For crystallization at higher supersaturation ($S_{e\text{-}w}$=3.5), after a rapid decrease in concentration with the appearance of crystals, the TB concentration remained a constant value of 14 mg/mL from 90 min to 180 min. Subsequently, the concentration further dropped and reached at a constant value of about 9.40 mg/mL after 240 min. Conversely, in the case of crystallization at lower supersaturation ($S_{e\text{-}w}$=2.7), TB concentration gradually decreased with time until it leveled off after 420 min.

(Fig. 2)

PXRD patterns of TB crystals obtained under various conditions are shown in Figure 3. It is apparent that the diffraction patterns of TB crystals obtained at the end of the crystallization from ethanol and ethanol-water with different supersaturation (2.7 and 3.5) are almost the same, giving the diffraction peaks typical for TB Form III crystals[24], e.g., 2θ=11.2°, 15.4° and 25.7°. By sharp contrast, the diffraction pattern of the TB crystals obtained at 90 min from ethanol-water with supersaturation of 3.5 (Fig. 3, wine line) is quite different from that of Form III , e.g., diffraction peaks typical for TB Form IV crystal[24] at 2θ=10.6°, 18.0°,18.8° and 27.0°. And the sample was stable at room temperature after two weeks, verified by PXRD analysis (Fig. 3, pink line). From the results above, it is found that only in the case of TB crystallization from ethanol-water at supersaturation of 3.5, TB crystallized into metastable Form IV firstly, which was consistent with Ostwald's Rule of Stages[41].

(Fig. 3)

The results of polarizing microscope showed that the crystalline polymorphs differed in habits. The morphology of Form III is needle-like (Fig. 4a, b, e and f), the same as Form III crystal habit in our previous work[28]. The morphology of Form IV is wheat-like (Fig. 4c), which were different from microfibril Form IV reported in our previous work[28] and thin needle-like Form IV reported by Tan and coworkers[26]. The photomicrograph of TB precipitated from ethanol-water ($S_{e\text{-}w}$=3.5) at 160 min (Fig. 4d) showed that some needle-like TB crystals were formed. When t=220 min, the wheat-like Form IV crystals were observed to fully transformed to needle-like Form

III (Fig. 4e).

(Fig. 4)

Figure 5 shows the comparison of FTIR spectra of Form III and Form IV TB crystals. It is found that the FTIR spectra of Form III obtained from ethanol and ethanol-water at the end of TB crystallization (red, black, blue and green line) are almost the same. The carbonyl stretching is observed at 1665 and 1663 cm^{-1} for Form III and Form IV, respectively, suggesting that carbonyl group is involved in a similar hydrogen bonding in these two polymorphs. The symmetric and asymmetric stretching frequencies of sulfonyl group are observed at 1342, 1166 cm^{-1} for Form III and 1348, 1166 cm^{-1} for Form IV. This suggests that sulfonyl group is involved in a stronger hydrogen bonding in Form III compared to Form IV. The IR absorption for the sulfonyl amide stretching is observed at 3331 and 3337 cm^{-1} for Form III and Form IV, respectively, which is consistent with the hydrogen bonding involving sulfonyl amide and carbonyl group. The methyl group (one at the end of the tail and another connected to aromatic group) stretching frequencies are observed at 2952, 2922 cm^{-1} for Form III and 2962, 2929 cm^{-1} for Form IV, respectively. Therefore, the peaks for the methyl group stretching of Form IV obviously shift towards higher wave number compared with those of Form III, indicating the conformational difference in the orientations of alkyl tail and aromatic ring in Form III and Form IV. The present FTIR spectra data is consistent with the work of Tan and coworkers[26], justifying the identification of TB polymorphs.

(Fig. 5)

From the results above, we could conclude that both supersaturation and solvents have great influence on the process of crystallization. To gain insight into the mechanism of competitive nucleation of TB at molecular level, we carried out Hirshfeld surface analysis of TB crystals and molecular dynamics simulation.

3.2. Hirshfeld surfaces analysis of TB polymorphs. According to the work of Tan and coworkers[26], TB conformers in the crystal structures can be divided into U–type (both the phenyl ring and alkyl tail are on the same side of the S–N1–C8–N2–C9 plane) and chair–type (both the phenyl ring and alkyl tail are on the opposite side of the S–N1–C8–N2–C9 plane). Based on the phenyl and alkyl tail orientation with respect to S–N1–C8–N2–C9 plane, Form I, III, IV and V adopt different U-type conformations (Fig. 6a), whereas Form II adopts four different chair type conformations (Ch1–Ch4) (Fig. 6b). And the molecular packing arrangements in different forms can be classified into four schemes (Fig. 6c): Both Forms I and III adopt the packing scheme A (the tolyl group and the butyl chain are on the opposite side of the urea tape in the structure), whereas both Form IV and V adopt packing scheme B (the tolyl group and the butyl chain are on the same side of the urea tape in the structure). As for Form II, Ch1 and Ch2 adopt packing scheme D, while Ch3 and Ch4 adopt packing scheme C and D.

(Fig. 6)

To explore the nature of intermolecular interactions in TB crystal structures, the Hirshfeld surface analysis of different TB polymorphs was carried out. Figure S1 shows surfaces that have been mapped over a d_{norm} range of -0.5–1.5 Å and the

associated 2D fingerprint plots. The large circular depressions (deep red) visible on the front and back views of the surfaces are indicative of hydrogen-bonding contacts, and other visible spots in the surfaces are due to H···H contacts.

Figure 7 contains the percentages of contributions for a variety of contacts in TB polymorphs. From these results, it can be seen that hydrogen bonds exist in all forms, and O···H/H···O interaction (28% - 30% of Hirshfeld surface) contribute significantly more than N···H/H···N interaction (2% - 5% of Hirshfeld surface). The proportions of O···H/H···O and N···H/H···N interaction are both maximum in TB Form I, consistent with the thermodynamically stable property of Form I. In addition, the C···C contacts, associated with π···π stacking interactions only exist in Forms IV (2.2% of Hirshfeld surface) and Form V (1.9% of Hirshfeld surface), and the minor contribution of C···C contacts (0.3% of Hirshfeld surface) in Form II can be neglected. These results offer us a rapid detection of TB crystal structures features through a "whole structure" view of intermolecular interactions and provide a foundation for the following TB nucleation study.

(Fig. 7)

3.3. Nucleation mechanism of TB in different conditions.

3.3.1. The structures of TB monomers in solution at 303 K. During the simulation time, TB molecules adjusted their conformation under the effect of solvents. Since TB molecules adopt different conformation in all the polymorphic forms[26], we calculated the average torsional angles of TB molecules in different solution at different initial concentration to explore the solvent effect on TB

conformation in solution and the relationship between TB conformation in solution and in final polymorphs.

In our simulations, seven torsion angles (τ_1 (C4–C5–S–N1), τ_2 (C5–S–N1–C8), τ_3 (S–N1–C8–N2), τ_4 (N1–C8–N2–C9), τ_5 (C8–N2–C9–C10), τ_6 (N2–C9–C10–C11), τ_7 (C9–C10–C11–C12), see Figure 1) were calculated by torsion distribution analysis. Since half molecules in TB crystals adopt τ_1–τ_7, while the other half molecules adopt the opposite torsion angles (-τ_1– -τ_7), we display only half for clarity. In the same way, for each torsion angle calculated in solution, the opposite values were neglected. As shown in Table 2, the torsional angles (τ_1–τ_7) of TB molecules in Form I changed different degrees due to the solute-solvent interaction. The most obvious variations occurred in τ_5 and τ_7, changing from gauche-conformation to anti-conformation. This is probably because the conformation change of alkyl tail of TB molecule has the lowest energy barrier[26] and anti-conformation is more stable than gauche-conformation due to smaller steric hindrance. For the same reason, τ_6 remained in anti-conformation. In the case of τ_2, τ_3 and τ_4, the torsional angles didn't change much, which could be attributed to the strong hydrogen bonds constraint between NH, O atoms of TB molecules and solvents. The torsional angles of the monomers in different solutions were quite similar with the only main difference in τ_1. At higher supersaturation, τ_1 resembled the corresponding torsional angle of Form IV molecules, whereas at lower supersaturation, τ_1 resembled the corresponding torsional angle of Form V molecules. After comparison, it is found that different solvents didn't have a great influence on the torsional angles of TB molecules. In addition, TB

conformers in both ethanol and ethanol-water solutions at 303 K were quite similar to Form IV molecules at higher supersaturation and Form V molecules at lower supersaturation, except that τ_5 was in anti-conformation instead of gauche-conformation.

(Table 2)

3.3.2. The formation of TB dimers in solution at 277 K. At the dimer level the nature of the associate and its intermolecular binding is an important factor in the nucleation process. And, the relationship between dimers formed in solution and dimers present in the final crystals needs to be explored. In our simulation at 277 K, TB aggregates were formed by both intermolecular hydrogen bonds and π ··· π interactions in all systems. Depending on the relative orientation of the TB molecules, there were mainly two types of TB dimers, as shown in Figure 8. One type is arranged with the tolyl group on the opposite side of the urea tape (Fig. 8a), which hereafter will be referred to as A-type dimers because they resemble the dimers in crystal Forms I and Form III. In the other type, however, tolyl groups are located on the same side of the urea tape (Fig. 8b), which resembles the packing mode of dimers in Form IV and Form V and will be referred to as B-type dimers. Two snapshots of the MD trajectories highlighting the presence of these two types of dimers are shown in Figure S2.

(Fig. 8)

The molecular structure of TB molecules in the solutions was analyzed via total and partial RDFs calculated from MD trajectories. The C-C (C refers to C2-C7) RDF

describes the relative intermolecular distance between the C atoms of the aromatic rings. The clear peak at ~4.1 Å evidences the formation of π-π stacking in solution (Fig. 9a). However, the total C-C RDF distribution does not allow us to distinguish B-type dimers with A-type dimers, so we studied the RDFs of individual C atoms. As shown in Figure 8, the intermolecular orientation of the TB molecules in A-type dimers with B-type dimers can be differentiated by analyzing C2-C2 and C5-C5 RDFs. In A-type dimers, a long-range order for the intermolecular C2-C2 distances around 9-12 Å and C5-C5 distance around 8-9 Å is expected. In contrast, the molecular orientation of the two TB molecules in B-type dimers would result in short distances at around 4-6 Å for each of the C2-C2 and C5-C5 partial RDFs. Thus, we can distinguish the formation of A-type dimers and B-type dimers through the analysis of the RDFs above. As seen in Figure 9b, two clear peaks for the C2-C2 RDFs can be observed in all systems. The first peak is at around 4.5-5 Å, which corresponds to C2-C2 distance of B-type dimers. And the second peak at around 9.5 Å can be regarded as C2-C2 distance of A-type dimer. However, C5-C5 RDFs (Fig. 9c) show only one intense peak at 5-6 Å for all systems. And a shoulder peak can be observed at ~ 9 Å for systems of S_e=2.7 and S_e =3.5, but not so obvious for systems of $S_{e\text{-}w}$=2.7 and $S_{e\text{-}w}$=3.5.

(Fig. 9)

Therefore, we defined a factor R as a reflection of the ratio of B-type dimers and A-type dimers by the following equation:

$$R = \frac{N_1}{N_2} = \frac{4\pi\rho\int_0^{r_1} r^2 g(r)dr}{4\pi\rho\int_{r_1}^{r_2} r^2 g(r)dr} = \frac{\int_0^{r_1} r^2 g(r)dr}{\int_{r_1}^{r_2} r^2 g(r)dr}$$

Where N_1 and N_2 is the coordination number obtained from the first peak and the second peak of C2-C2 RDF plot, respectively. In this case, r_1 is around 7.5 Å and r_2 is around 11.4 Å. Since the density is the same for one RDF plot, R can be simplified without the influence of density.

Table 3 lists the results of R values calculated in different period of simulation time. For crystallization from ethanol, R is always smaller than unity, demonstrating the predominant existence of A-type dimers. And as the simulation proceeds, R values decrease a little (within 0.2), which means the ratio of A-type dimers increase. In the last 1 ns, A-type dimers formed in solution are almost twice as many as B-type dimers. Thus, the predominant A-type dimers may lead to the nucleation of Form I or Form III. For crystallization from ethanol-water at $S_{e\text{-}w}$=2.7, R increases significantly during 1-2 ns and then drops to 0.89 in 3-4 ns, so A-type dimers are slightly more than B-type dimers, which may lead to the nucleation of Form I or Form III. While at $S_{e\text{-}w}$=3.5, a dramatic increase of R is observed from 2 to 4 ns, and the value (1.83) in the end of the simulation is much larger than unity, so the nucleation of Form IV or Form V may occur due to the predominant B-type dimers. Because the monomers in solution of $S_{e\text{-}w}$=3.5 system resembled Form IV molecules most, we took the energy of Form IV molecules as E_{TB} to calculate the binding energy of TB dimers. It is found that the binding energy of Form IV dimers are -82.26 kJ/mol, higher than that of Form V dimers (-77.48 kJ/mol). Therefore, it is easier for monomers in solutions to form

dimers of Form IV than to form dimers of Form V. This is probably why Form IV could be obtained from ethanol-water at initial supersaturation of 3.5. A typical dimer formed in $S_{e\text{-}w}$=3.5 system is shown in Figure 8b. TB molecules form π···π stacking with C2-C2 distance of 5.57 Å and C5-C5 distance of 5.81 Å, compared with the corresponding distances of 5.62 Å and 6.18 Å in dimers of Form IV crystal. The intermolecular N1H···O3, N2H···O3 and N2H···O1 hydrogen bond distance are 1.93, 2.39 and 2.31 Å, respectively, which are quite close to the counterpart in dimers of Form IV crystal (1.96, 2.40 and 2.35 Å).

(Table 3)

As the simulation proceeded, the dimers in all systems began to aggregate and form clusters (the aggregate containing at least three TB molecules are considered to be a cluster). The time for the formation of TB clusters was about 500, 750, 1250 and 1750 ps for systems of S_e=3.5, S_e=2.7, $S_{e\text{-}w}$=3.5 and $S_{e\text{-}w}$=2.7, respectively, indicating that higher supersaturation contributes to the decrease of nucleation time. Figure S3 shows the TB clusters formed in each system at the end of the simulation. It was observed that 15，11，6 and 4 TB molecules were included in the biggest clusters in the systems of S_e=3.5, S_e=2.7, $S_{e\text{-}w}$=3.5 and $S_{e\text{-}w}$=2.7, respectively.

3.3.3. TB-solvent interactions and TB-TB interactions in solution. Since the competitive relationship between solute-solute and solute-solvents can largely influence the nucleation process and the polymorph outcome, it is important to investigate the TB-TB interactions and TB-solvents interactions in solution.

There are eight kinds of hydrogen bonds formed between TB and solvents,

namely, O1(O2)⋯He, O1(O2)⋯Hw, O3⋯He, O3⋯Hw, N1H⋯Oe, N1H⋯Ow, N2H⋯Oe, N2H⋯Ow (The atomic names were defined in Figure 1). The formation of hydrogen bonds between TB and solvents under various conditions are indicated by the differences in RDFs for TB and solvents atoms (Fig. S4). The length of hydrogen bond was set to be less than 4 Å, so only the first peak is taken into account. From the results of RDFs of O-Hs and NH-Os (O refers to O1, O2 and O3, Hs refers to He and Hw, NH refers to N1H and N2H, Os refers to Oe and Ow), it is found that the first peak in O-He and O-Hw RDFs is at 1.75 Å and 1.85 Å, respectively, showing that O⋯He bond length is shorter than O⋯Hw bond length. Thus, O⋯He bonds are stronger than O⋯Hw bonds. NH-Oe and NH-Ow RDFs show broader peaks at 2.15 Å and 2.25 Å respectively, showing that NH⋯Os bonds are weaker than O⋯Hs bonds. Considering the positions of the peaks for the same hydrogen bond of different systems are the same, the hydrogen bond interactions are mainly reflected in coordination number (Table 4), which represents the number of hydrogen bonds formed between TB and solvents. For crystallization from ethanol, the coordination number of O⋯He and NH⋯Oe both decrease as the initial supersaturation increases, demonstrating more hydrogen bonds are formed in system with lower initial supersaturation. And for crystallization from ethanol-water, the coordination number of O⋯He, NH⋯Oe and NH⋯Ow all increase as the initial supersaturation increases, and the coordination number of O⋯Hw is the same for both systems. Thus, more hydrogen bonds are formed in system with higher initial supersaturation. In addition, the coordination number of TB-ethanol hydrogen bonds is bigger than that of

TB-water hydrogen bonds, indicating that TB molecules bind to more ethanol molecules than water molecules.

(Table 4)

For crystallization from ethanol, the binding energy of TB-solvent is -162.43 kJ/mol and -169.03 kJ/mol for S_e=3.5 and 2.7 systems, separately. Thus, the binding interaction between TB and solvent is stronger in system with the lower initial supersaturation. In contrast, for crystallization from ethanol-water, system with the higher initial supersaturation results in a more favorable interaction between TB and solvent (-186.62 kJ/mol), compared to system with the lower initial supersaturation (-175.95 kJ/mol). It is interesting to note that the order of TB-solvent interaction in different systems is the same as that of *R* factor, that is, solution with stronger TB-solvent interaction has more B-type dimers than A-type dimers. Therefore, B-type dimers are predominant in $S_{e\text{-}w}$=3.5 system which has the strongest TB-solvent interaction, and thus leads to the formation of Form IV crystals.

The intermolecular hydrogen bonds of TB molecules contribution to aggregation of TB molecules were also studied by NH-O RDFs. As seen from Figure S4, a clear peak is at 2.05 Å for all systems, indicating no difference for hydrogen bond length. In addition, the peak of $g_{NH\text{-}O}$ gives coordination numbers of 0.89, 0.66, 0.33 and 0.63 for systems of S_e=3.5, S_e=2.7, $S_{e\text{-}w}$=3.5 and $S_{e\text{-}w}$=2.7, respectively (Table 4). The order of the results above is opposite to the binding interaction of TB and solvents. That is, the system with higher TB-solvents binding energy has less TB-TB intermolecular hydrogen bonds and higher *R* value. Therefore, we can conclude that strong hydrogen

bonds interaction between TB and solvents prevent the formation of intermolecular hydrogen bonds of TB molecules. Thus, TB molecules aggregate by π···π interaction to make up the loss of intermolecular TB-TB hydrogen bonds. That is why most B-type dimers appear in crystallization from ethanol-water with supersaturation of 3.5 and lead to the formation of Form IV.

By comparison with our previous work[28] and Uekama's work[29], we can find that the premise for the preferential growth of TB Form IV crystals is strong interaction between TB and surrounding molecules, including solvents, self-assembled monolayers, as well as additives. This strong interaction can induce and stabilize the metastable crystal in solution, postponing or even inhibiting the solution-mediated transformation of the metastable form to the stable form.

CONCLUSIONS

The rapid-cooling crystallization of tolbutamide from ethanol and ethanol-water at different initial supersaturations (3.5 and 2.7) were studied through characterizations of PXRD and crystals morphologies. It is found that crystallization from ethanol resulted in only the stable Form III under both supersaturations. However, from ethanol-water solution at higher initial supersaturation, the highest bioavailable TB crystals of metastable Form IV were obtained. The experiments results are well explained by competitive relationship between solute-solute and solute-solvent interaction using theoretical method. Hirshfeld surface analysis and the associated 2D fingerprint plots of five TB polymorphs clearly quantify the interactions within the crystal structures, revealing π···π interaction only exist in Form IV and Form V. MD

simulation shows the stronger hydrogen bonds interactions between TB and solvents in ethanol-water at higher supersaturation weaken the TB-TB intermolecular NH···O hydrogen bonds and thus promote TB molecules to form dimers by π···π stacking, which is the main characteristic of Form IV and Form V dimers. Binding energy calculation of TB dimers indicates the formation of Form IV dimers is easier than that of Form V dimers. This work discloses the reason for the formation of metastable TB crystals at specific condition and sheds light on the selective crystallization of organic crystal polymorphs by simply controlling the solvents and supersaturations.

Acknowledgements

This work was supported by NSFC (21106094, 20836005, 21076141), RFDP (20100032120015) and Tianjin Science Foundation for Youths, China (12JCQNJC03100).

References

1 L. F. Huang and W. Q. Tong, *Adv. Drug Delivery Rev.*, 2004, **56**, 321-334.
2 A. R. Sheth, S. Bates, F. X. Muller and D. J. W. Grant, *Cryst. Growth Des.*, 2004, **4**, 1091-1098.
3 M. Kitamura and S. Hironaka, *Cryst. Growth Des.*, 2006, **6**, 1214-1218.
4 D. Deng, L. Liu, B.-M. Ji, G. Yin and C. Du, *Cryst. Growth Des.*, 2012, **12**, 5338-5348.
5 C. Sudha and K. Srinivasan, *CrystEngComm*, 2013, **15**, 1914-1921.
6 W. Y. Su, H. X. Hao, B. Glennon and M. Barrett, *Cryst. Growth Des.*, 2013, **13**, 5179-5187.
7 W. Du, Q. Yin, Y. Bao, C. Xie, B. Hou, H. Hao, W. Chen, J. Wang and J. Gong, *Ind. Eng. Chem. Res.*, 2013, **52**, 16182-16189.
8 A. Kupka, V. Vasylyeva, D. W. M. Hofmann, K. V. Yusenko and K. Merz, *Cryst. Growth Des.*, 2012, **12**, 5966-5971.
9 M. Kitamura and K. Horimoto, *J. Cryst. Growth*, 2013, **373**, 151-155.
10 L. Xu, X. Miao, B. Zha and W. Deng, *J. Phys. Chem. C*, 2012, **116**, 16014-16022.
11 O. Narducci and A. G. Jones, *Cryst. Growth Des.*, 2012, **12**, 1727-1735.
12 W. Liu, H. Wei, J. Zhao, S. Black and C. Sun, *Org. Process Res. Dev.*, 2013, **17**, 1406-1412.
13 B. Ji, M. Cusack, A. Freer, P. S. Dobson, N. Gadegaard and H. Yin, *Integrative Biology*, 2010, **2**, 528-535.
14 V. Lopez-Mejias, J. L. Knight, C. L. Brooks and A. J. Matzger, *Langmuir*, 2011, **27**, 7575-7579.
15 E. A. Losev, M. A. Mikhailenko, A. F. Achkasov and E. V. Boldyreva, *New Journal of Chemistry*,

2013, **37**, 1973-1981.
16 J.-P. Brog, C.-L. Chanez, A. Crochet and K. M. Fromm, *RSC Advances*, 2013, **3**, 16905-16931.
17 A. S. Myerson and B. L. Trout, *Science*, 2013, **341**, 855-856.
18 S. Hamad, C. Moon, C. R. A. Catlow, A. T. Hulme and S. L. Price, *J. Phys. Chem. B*, 2006, **110**, 3323-3329.
19 J. Chen and B. L. Trout, *J. Phys. Chem. B*, 2008, **112**, 7794-7802.
20 L. Tavagnacco, U. Schnupf, P. E. Mason, M.-L. Saboungi, A. Cesàro and J. W. Brady, *J. Phys. Chem. B*, 2011, **115**, 10957-10966.
21 Y. Yani, P. S. Chow and R. B. H. Tan, *Cryst. Growth Des.*, 2012, **12**, 4771-4778.
22 S. Chattopadhyay, D. Erdemir, J. M. B. Evans, J. Ilavsky, H. Amenitsch, C. U. Segre and A. S. Myerson, *Cryst. Growth Des.*, 2005, **5**, 523-527.
23 R. J. Davey, N. Blagden, S. Righini, H. Alison, M. J. Quayle and S. Fuller, *Cryst. Growth Des.*, 2000, **1**, 59-65.
24 K. Kimura, F. Hirayama and K. Uekama, *J. Pharm. Sci.*, 1999, **88**, 385-391.
25 G. Hasegawa, T. Komasaka, R. Bando, Y. Yoshihashi, E. Yonemochi, K. Fujii, H. Uekusa and K. Terada, *Int. J. Pharm.*, 2009, **369**, 12-18.
26 S. Thirunahari, S. Aitipamula, P. S. Chow and R. B. H. Tan, *J. Pharm. Sci.*, 2010, **99**, 2975-2990.
27 N. K. Nath and A. Nangia, *CrystEngComm*, 2011, **13**, 47-51.
28 J. L. Zhang, A. Y. Liu, Y. Han, Y. Ren, J. B. Gong, W. Li and J. K. Wang, *Cryst. Growth Des.*, 2011, **11**, 5498-5506.
29 Y. Sonoda, F. Hirayama, H. Arima, Y. Yamaguchi, W. Saenger and K. Uekama, *Cryst. Growth Des.*, 2006, **6**, 1181-1185.
30 G. Hou, Q. Yin, M. Zhang, W. Su, H. Mao and J. Wang, *J. Chem. Eng. Data*, 2009, **54**, 2106-2108.
31 M. A. Spackman and P. G. Byrom, *Chem. Phys. Lett.*, 1997, **267**, 215-220.
32 J. J. McKinnon, A. S. Mitchell and M. A. Spackman, *Chem.—Eur. J.*, 1998, **4**, 2136-2141.
33 S. K. Wolff, D. J. Grimwood, J. J. McKinnon, M. J. Turner, D. Jayatilaka and M. A. Spackman, CRYSTAL EXPLORER, version 3.1, University of Western Australia, Perth, Australia, 2012.
34 P. Dauger-Osguthorpe, V. A. Roberts, D. J. Osguthorpe, J. Wolff, M. Genest and A. T. Hagler, *Proteins: Struct., Funct., Genet.*, 1988, **4**, 21.
35 J. R. Hill, A. R. Minihan, E. Wimmer and C. J. Adams, *Phys. Chem.Chem. Phys.*, 2000, **2**, 4255-4264.
36 W. G. Hoover, *Physical Review A*, 1985, **31**, 1695-1697.
37 P. P. Ewald, *Annales de Physique*, 1921, **64**, 253.
38 S. Hamad, C. E. Hughes, C. R. A. Catlow and K. D. M. Harris, *J. Phys. Chem. B*, 2008, **112**, 7280-7288.
39 J. Anwar and D. Zahn, *Angew. Chem.-Int. Edit.*, 2011, **50**, 1996-2013.
40 L. Gomez-Hortiguela, S. Hamad, F. Lopez-Arbeloa, A. B. Pinar, J. Perez-Pariente and F. Cora, *J. Am. Chem. Soc.*, 2009, **131**, 16509-16524.
41 W. Ostwald, *Z. Phys. Chem*, 1897, **22**, 289-330.

Table 1. Molecular Dynamics Simulation Details

supersaturation	number of molecules	density of systems (g/cc)	simulated cell size (Å)
S_e=3.5[a]	N_{TB}:$N_{ethanol}$=16:484	0.945	36.03*36.03*36.02
S_e=2.7	N_{TB}:$N_{ethanol}$=12:488	0.909	36.07*36.07*36.07
$S_{e\text{-}w}$=3.5 [b]	N_{TB}:$N_{ethanol}$:N_{H2O}=8:700:1132	0.895	48.21*48.21*48.21
$S_{e\text{-}w}$=2.7	N_{TB}:$N_{ethanol}$:N_{H2O}=6:680:1102	0.887	48.28*48.28*48.28

[a] S_e represents the supersaturation of system using ethanol as solvent. [b] $S_{e\text{-}w}$ represents the supersaturation of system using ethanol-water as solvent.

Table 2. The average torsion angles (°) of TB molecules calculated under various conditions at 303 K.

	τ_1	τ_2	τ_3	τ_4	τ_5	τ_6	τ_7
S_e=3.5	105	69	-178	-177	-176	-177	178
S_e=2.7	89	62	-179	-178	-176	-177	176
$S_{e\text{-}w}$=3.5	101	70	-179	-179	-177	-178	179
$S_{e\text{-}w}$=2.7	89	70	-179	-176	-177	-177	179
Form I[a]	141.9	-50.8	147.6	-174.3	81.5	-178.8	-69.3
Form IV [a]	94.3	63.2	-154.3	-174.4	-85.7	-179.3	162.6
Form V [a]	89.4	64.2	-166.4	178.9	-85.1	-176.1	-176.1

[a] The torsional angles of Form I, IV and V are obtained from the work of Tan[26] and Nangia[27].

Table 3. The values of R in different period of simulation time at T=277 K.

	0-1 ns	1-2 ns	2-3 ns	3-4 ns
S_e=3.5	0.60	0.64	0.60	0.47
S_e=2.7	0.73	0.70	0.61	0.56
$S_{e\text{-}w}$=3.5	0.51	0.53	1.09	1.83
$S_{e\text{-}w}$=2.7	0.45	0.99	1.12	0.89

Table 4. Coordination number for TB-Solvents and TB-TB hydrogen bonds under various conditions at T=277 K.

	TB-Solvents				TB-TB
	O-He	O-Hw	NH-Oe	NH-Ow	NH-O
S_e=3.5	0.64		1.11		0.89
S_e=2.7	0.72		1.21		0.66
$S_{e\text{-}w}$=3.5	0.56	0.09	1.12	0.23	0.33
$S_{e\text{-}w}$=2.7	0.48	0.09	0.96	0.15	0.63

Captions for Figures

Fig. 1 Molecular structures of TB, water and ethanol. The atomic numbering and types in each molecule were also defined here.

Fig. 2 Change in concentration of TB in the crystallization (a) from ethanol at the supersaturation of 3.5 (black line) and 2.7 (red line); (b) from ethanol-water solution at the supersaturation of 3.5 (black line) and 2.7 (red line).

Fig. 3 PXRD patterns of TB crystals obtained under various conditions.

Fig. 4 Photomicrographs of TB crystals precipitated from (a) ethanol at the supersaturation of 3.5 (sampled at the end), (b) ethanol at the supersaturation of 2.7 (sampled at the end), (c) ethanol-water at the supersaturation of 3.5 (sampled at 90 min),(d) ethanol-water at the supersaturation of 3.5 (sampled at 160 min), (e) ethanol-water at the supersaturation of 3.5 (sampled at the end), (f) ethanol-water at the supersaturation of 2.7 (sampled at the end). (all pictures were magnified 50 times)

Fig. 5 FTIR spectra of Form III and Form IV crystals of TB. (red line: S_e=3.5, sampled at the end; black line: S_e=2.7 sampled at the end; blue line: $S_{e\text{-}w}$=3.5, sampled at the end; green line: $S_{e\text{-}w}$=2.7, sampled at the end; purple line: $S_{e\text{-}w}$=3.5, sampled at t=90 min)

Fig. 6 Overlay of conformers observed in TB Forms I and III–V (red—U1 (Form I); green—U2 (Form III); brown—U3 (Form IV); violet—U4 (Form V)) (a), Form II (pink—Ch1, yellow—Ch2, light blue—Ch3, thick blue—Ch4) (b). (c) Types of packing schemes in TB polymorphs.

Fig. 7 Relative contributions of various intermolecular contacts to the Hirshfeld surface area in TB Forms I –V (Ch2 and Ch4 in Form II are not shown due to similarity of Ch1 and Ch2, Ch3 and Ch4).

Fig. 8 Illustration of the types of dimers that the TB molecules can form in the simulation. Dimers

taken from (a) S_e=2.7 system at t=1202 ps; (b) $S_{e\text{-}w}$=3.5 system at t=3402 ps. (The blue dashed lines represent hydrogen bonds)

Fig. 9 RDFs for (a) C-C (b) C2-C2 (c) C5-C5 interactions under different conditions in 3-4 ns.

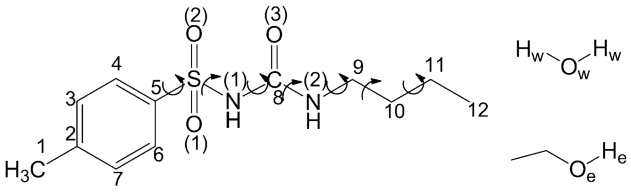

Fig. 1

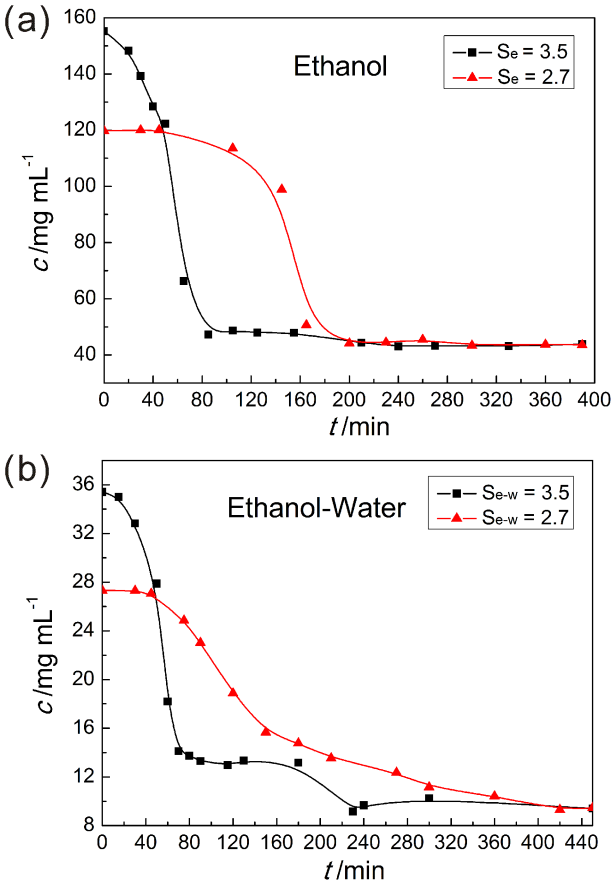

Fig. 2

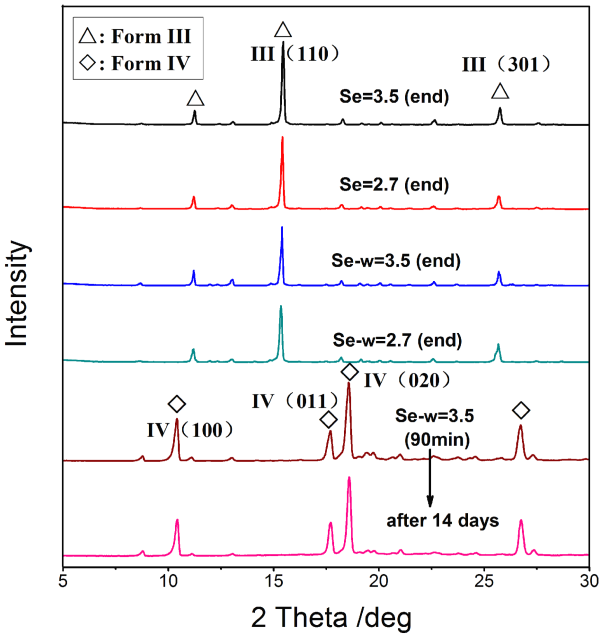

Fig. 3

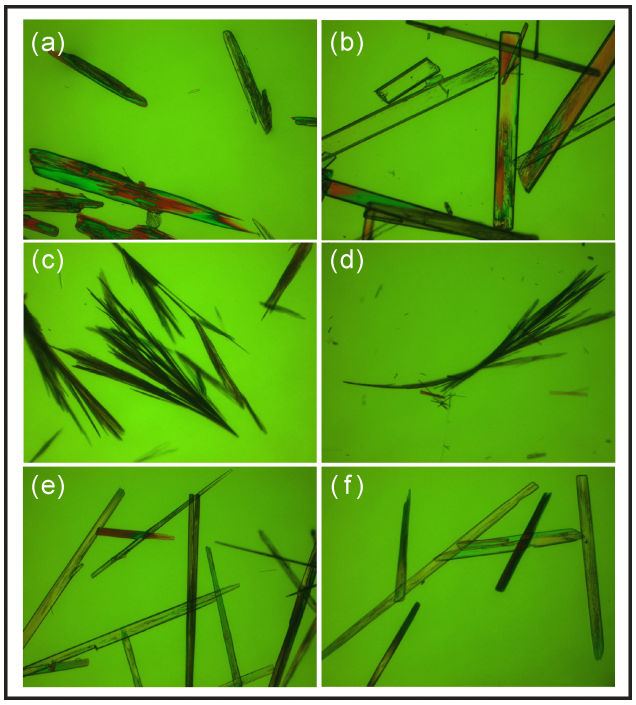

Fig. 4

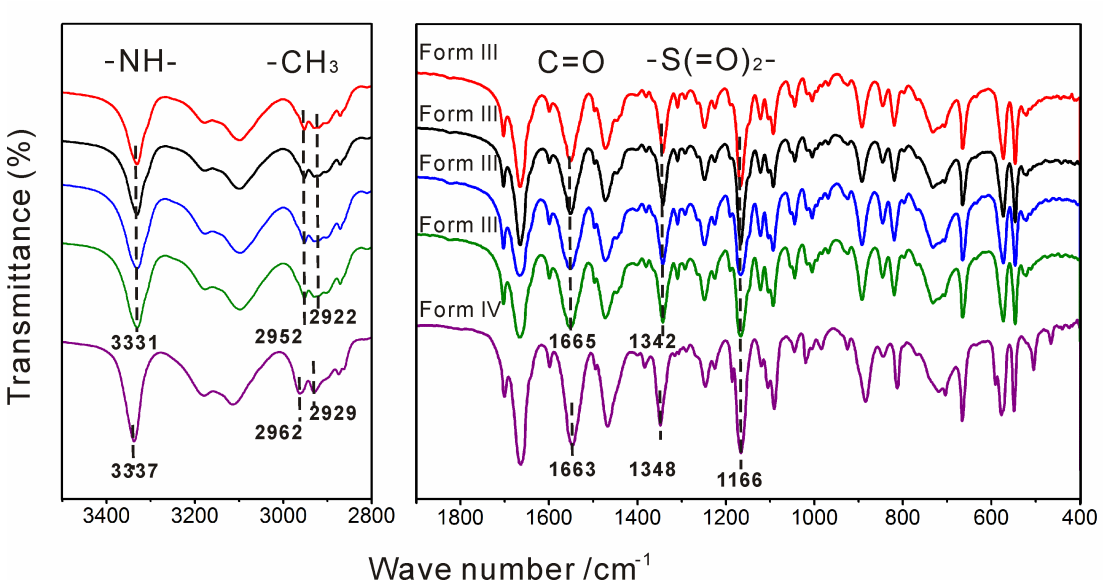

Fig. 5

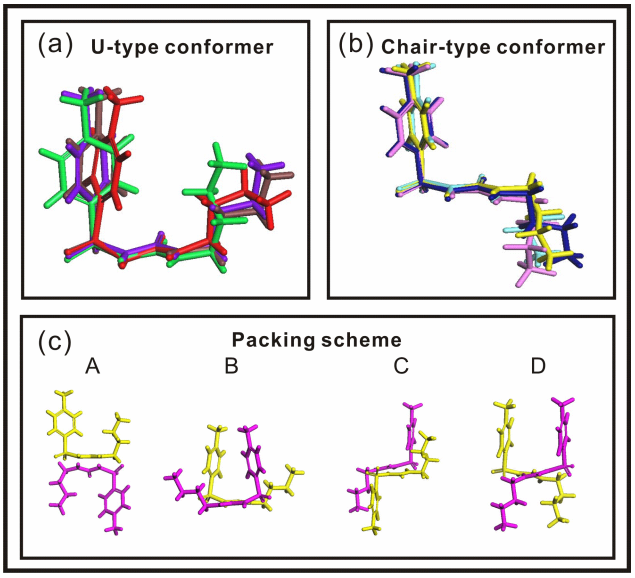

Fig. 6

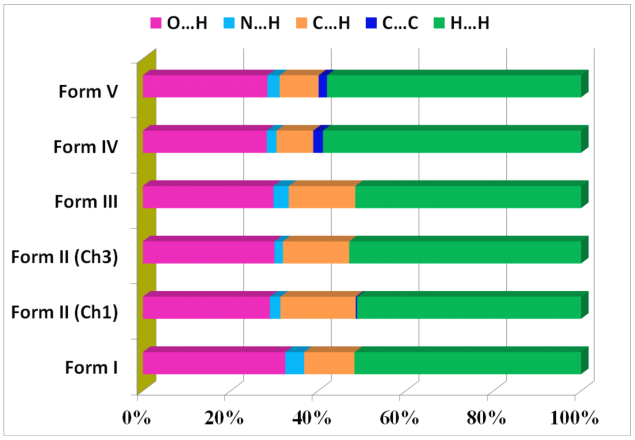

Fig. 7

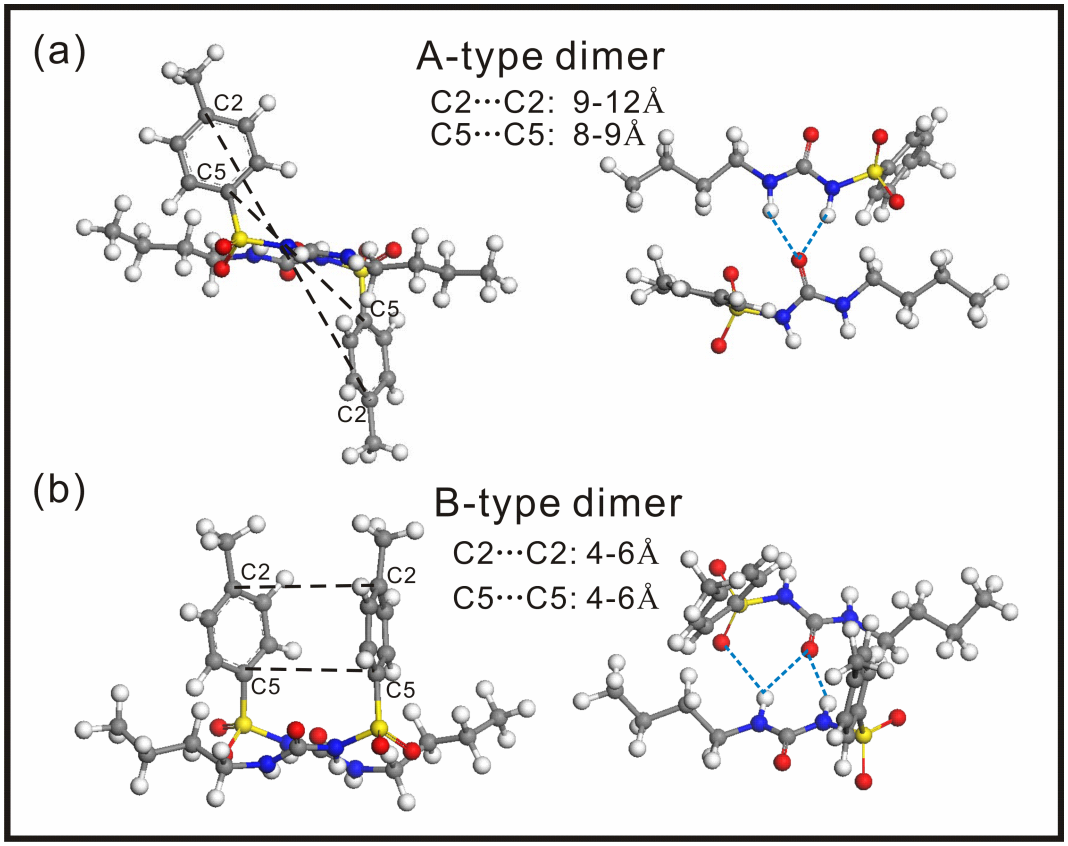

Fig. 8

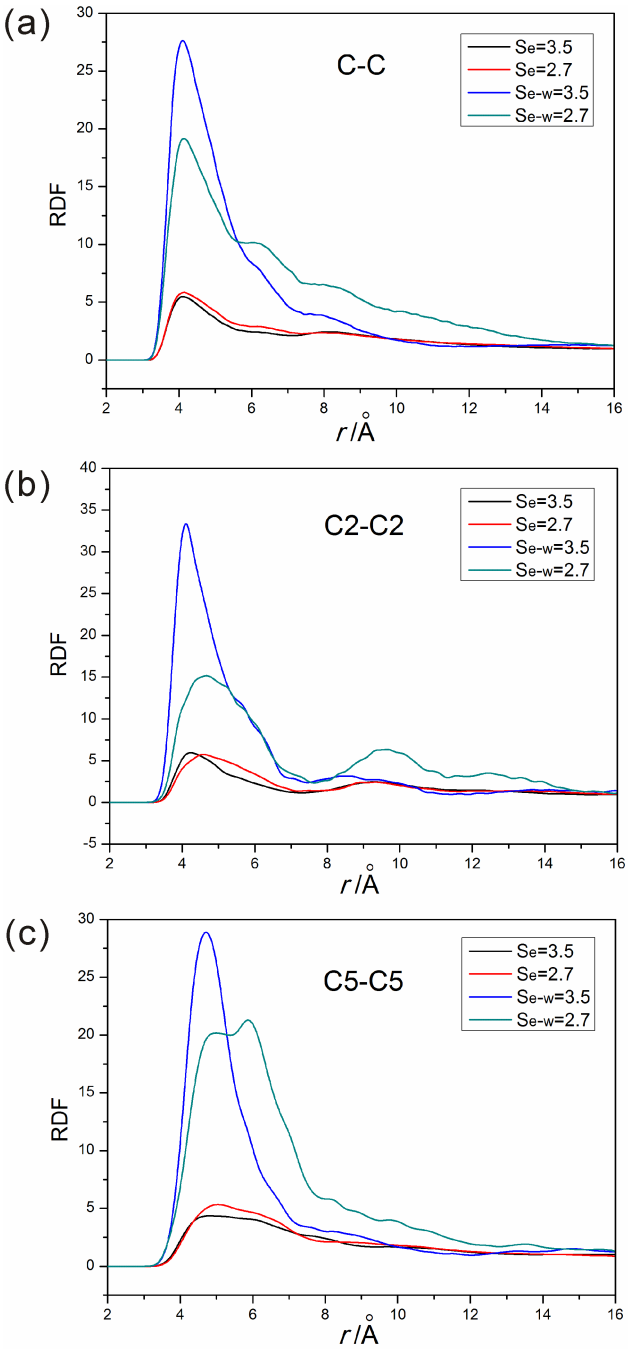

Fig. 9